GoAmazon2014/5 campaign points to deep-inflow approach to deep convection across scales

Kathleen A. Schiro[a,b,1], Fiaz Ahmed[a], Scott E. Giangrande[c], and J. David Neelin[a]

[a]Department of Atmospheric and Oceanic Sciences, University of California, Los Angeles, CA 90095; [b]Jet Propulsion Laboratory, California Institute of Technology, Pasadena, CA 91109; and [c]Environmental and Climate Sciences Department, Brookhaven National Laboratory, Upton, NY 11967

Edited by Kerry A. Emanuel, Massachusetts Institute of Technology, Cambridge, MA, and approved March 20, 2018 (received for review November 14, 2017)

A substantial fraction of precipitation is associated with mesoscale convective systems (MCSs), which are currently poorly represented in climate models. Convective parameterizations are highly sensitive to the assumptions of an entraining plume model, in which high equivalent potential temperature air from the boundary layer is modified via turbulent entrainment. Here we show, using multiinstrument evidence from the Green Ocean Amazon field campaign (2014–2015; GoAmazon2014/5), that an empirically constrained weighting for inflow of environmental air based on radar wind profiler estimates of vertical velocity and mass flux yields a strong relationship between resulting buoyancy measures and precipitation statistics. This deep-inflow weighting has no free parameter for entrainment in the conventional sense, but to a leading approximation is simply a statement of the geometry of the inflow. The structure further suggests the weighting could consistently apply even for coherent inflow structures noted in field campaign studies for MCSs over tropical oceans. For radar precipitation retrievals averaged over climate model grid scales at the GoAmazon2014/5 site, the use of deep-inflow mixing yields a sharp increase in the probability and magnitude of precipitation with increasing buoyancy. Furthermore, this applies for both mesoscale and smaller-scale convection. Results from reanalysis and satellite data show that this holds more generally: Deep-inflow mixing yields a strong precipitation–buoyancy relation across the tropics. Deep-inflow mixing may thus circumvent inadequacies of current parameterizations while helping to bridge the gap toward representing mesoscale convection in climate models.

tropical precipitation | moist convection | mesoscale convective system | convective parameterization | entrainment

Convective parameterizations in climate and numerical weather prediction models are commonly built around the assumptions of an entraining plume model (1–4) for the incorporation of environmental air into cumulonimbus updrafts. Representation of entrainment remains a matter of debate (see ref. 5 for review), introducing poorly constrained parameter sensitivity in general circulation models (GCMs). This affects simulation of tropical climate (6, 7) and contributes to uncertainty in global warming projections (8–11).

Deep convective cumulonimbus can exist in isolation or can aggregate to give rise to mesoscale convective systems (MCSs) (12). MCSs in the tropics play a substantial role in redistribution of heat (13, 14) and momentum (15). Currently, most convective parameterizations do not take MCSs into account despite arguments for their inclusion (16–18), including their ubiquity (19) and their contributions to total rainfall (20) and variability (21, 22). The distinguishing features of mesoscale convection—including organized inflow and outflow structures (23–25)—are excluded in entraining plume subgrid-scale representations and are too fine to be resolved at a typical GCM resolution, thereby falling through the cracks of computational compromises. It will be many years before centennial-scale simulations for effects of anthropogenic climate change are routinely conducted with resolutions that explicitly resolve convection (26). In the meantime, observational groundwork for incorporating key aspects of subgrid organization is essential.

Here we seek a formulation of entrainment that is observationally more representative of mesoscale convection and to assess the extent to which this can reproduce observed precipitation statistics. In mass continuity terms, the question of lateral entrainment hinges on how much environmental mass flows into the updraft as a function of altitude (27). Field observations suggest that the flow can be highly organized in mesoscale systems (28–30), and modeling studies (30–32) indicate that deep convective systems often have a deep layer of environmental air (sometimes about 4–5 km thick) flowing into their updrafts through the lower free troposphere, with most of the air originating above cloud base (31, 32). A "deep-inflow" formulation of mixing that emphasizes the layer through which the environment affects the updraft (33) can potentially treat coherent and smaller-scale turbulent inflow on a compatible basis.

Both observational (33–36) and modeling (37) studies have suggested that the transition to deep convection is highly sensitive to the availability of moisture in the lower free troposphere, thus explaining the observed precipitation–column-water-vapor relation (33, 36, 38–43). Previous efforts have indicated that the observed sharp increase in precipitation as a function of column water vapor is associated with effects of air entrained in the lower troposphere (33, 36). There is thus a need to connect observational constraints on updrafts with a mixing formulation that can

Significance

Representations of strongly precipitating deep-convective systems in climate models are among the most important factors in their simulation. Parameterizations of these motions face the dual challenge of unclear pathways to including mesoscale organization and high sensitivity of convection to approximations of turbulent entrainment of environmental air. Ill-constrained entrainment processes can even affect global average climate sensitivity under global warming. Multiinstrument observations from the Department of Energy GoAmazon2014/5 field campaign suggest that an alternative formulation from radar-derived dominant updraft structure yields a strong relationship of precipitation to buoyancy in both mesoscale and smaller-scale convective systems. This simultaneously provides a key step toward representing the influence of mesoscale convection in climate models and sidesteps a problematic dependence on traditional entrainment rates.

Author contributions: K.A.S. and J.D.N. designed research; K.A.S., F.A., and J.D.N. performed research; K.A.S., F.A., and S.E.G. analyzed data; and K.A.S., F.A., and J.D.N. wrote the paper.

The authors declare no conflict of interest.

This article is a PNAS Direct Submission.

Data deposition: The GoAmazon2014/5 data can be downloaded at the ARM data archive (https://www.arm.gov/data). TRMM 3B42 data are disseminated by the Goddard Earth Sciences Data and Information Services Center (https://pmm.nasa.gov/data-access/downloads/trmm). ERA-Interim reanalysis products are available through the European Centre for Medium-Range Weather Forecasts (apps.ecmwf.int/datasets/data/interim-full-daily/levtype=sfc/).

[1]To whom correspondence should be addressed. Email: kathleen.a.schiro@jpl.nasa.gov.

This article contains supporting information online at www.pnas.org/lookup/suppl/doi:10.1073/pnas.1719842115/-/DCSupplemental.

Published online April 17, 2018.

predict precipitation onset as a function of plume buoyancy for GCM parameterization.

In this study, the multiple instruments at the Department of Energy Atmospheric Radiation Measurement (DOE ARM) GoAmazon2014/5 site (44) permit a coordinated assessment of the following: (*i*) direct estimates of updraft mass flux and implications for mixing and (*ii*) evaluation of the relation between updraft buoyancy derived under this deep-inflow mixing and deep convective onset for both convection that meets mesoscale spatial criteria and smaller-scale convection. The robustness of these results is tested across tropical land and ocean regions, using reanalysis and remote-sensing data.

Updraft Mass Flux in Mesoscale and Smaller-Scale Convection at GoAmazon2014/5

Profiles of increasing vertical velocity and mass flux with height suggest large lower-tropospheric inflow into an updraft. Initial empirical evidence of deep-inflow structure in deep convective updrafts stems from aircraft sampling of MCSs in field campaigns over tropical ocean (e.g., ref. 45). Mean characteristics of convective updrafts from radar wind profilers (RWPs) have shown consistency with field campaign observations and across land and ocean sites (46–48). We examine updraft mass flux separately for mesoscale systems and for convection occurring at smaller spatial scales and ask whether characteristics suggestive of deep-inflow mixing are sufficiently consistent such that a single framework for mixing in GCMs can apply to deep convection occurring in both ranges of spatial scale.

Radar Vertical Velocity. RWP retrievals of vertical velocity from the GoAmazon2014/5 site (as described in ref. 48) are analyzed for deep convective events. Hydrometeor fall speed contributions are accounted for as in ref. 49. Data are averaged into 1-min intervals for our analysis here.

To ensure sampling of deep convective updrafts, criteria are imposed for convection, depth, and strength of vertical velocity: (*i*) The convection criterion of ref. 48 is applied, which uses a fuzzy logic-based classifier that relies on reflectivity, mean Doppler velocity, bright-band signatures, and texture parameters (49). (*ii*) The depth criterion ensures that the updrafts sampled extend from low levels to the upper troposphere (>9 km) by requiring that 1-min profiles have positive layer-mean vertical velocities in all of 0–3 km, 3–6 km, 6–9 km, and 9–12 km. The 9- to 12-km layer can be positive immediately before or after the sampled profile meeting all other criteria, to include cores tilted in height with time. (*iii*) The strength criterion demands that $\geq$10% of each vertical profile contains vertical velocities >1 ms^{-1}. Sensitivity tests confirm that the results in Fig. 1 are robust to modifying this threshold (Fig. S2).

Updraft events are then identified from contiguous 1-min mean profiles meeting these criteria. We are interested in average mass flux, especially in the lower troposphere. Each event typically contains high vertical velocities at some times and heights (about 30% of profiles exceed 5 $m{\cdot}s^{-1}$ at some height), but note that the updraft mass flux also contains a substantial contribution from motions <1 ms^{-1} (at least half the profile in 50% of the samples). Fig. 1*A* is an example of a strong convective event with updraft maximum ≈20 ms^{-1} (50, 51). Fig. 1*B* shows the mean vertical velocity of all events, smoothed with a running mean (window length 0.5 km), with the 90th percentile of all 1-min mean profiles indicating the range of strong upward velocities within the events. Vertical velocity increases nearly linearly with height throughout the entire lower troposphere up to the point where data retrievals near the melting level are masked out (49). This translates to a mass flux (Fig. 1*C*) increasing approximately linearly in height throughout the lower troposphere as calculated from $m = \rho\sigma w$, where ρ is a mean density profile from radiosonde data, w is the mean vertical velocity, and σ is estimated simply by the fraction $n_{conv}(z)/N$, where n_{conv} is the number of points satisfying the updraft criteria. The normalization N does not affect the vertical structure used for mixing estimates (here N is profiles with any radar echo present; for mass flux averaged over the entire observation period, multiply m by 0.11). Alternate definitions yield similar results (47, 48). These results are consistent with studies establishing RWP methodology (47, 48) and field campaign observations of large convective systems over tropical oceans (29, 30).

Updraft Mass Flux in Mesoscale and Smaller-Scale Convection. To compare mean updraft characteristics of mesoscale and smaller-scale convection, a second radar (S band) is used to identify systems within a 100-km domain surrounding the GoAmazon2014/5 site (*Materials and Methods*). Mesoscale systems follow a traditional definition of having a region of contiguous pixels of composite radar reflectivity >20 dBZ (in decibel units relative to 1 $mm^6\ m^{-3}$) extending 100 km or greater in any direction (12), with a maximum of 45 dB dBZ or greater. We use the term "smaller-scale convection" to denote events that likewise have a maximum exceeding 45 dBZ, but with the 20-dBZ region less than 50 km in its longest direction. Events with maximum

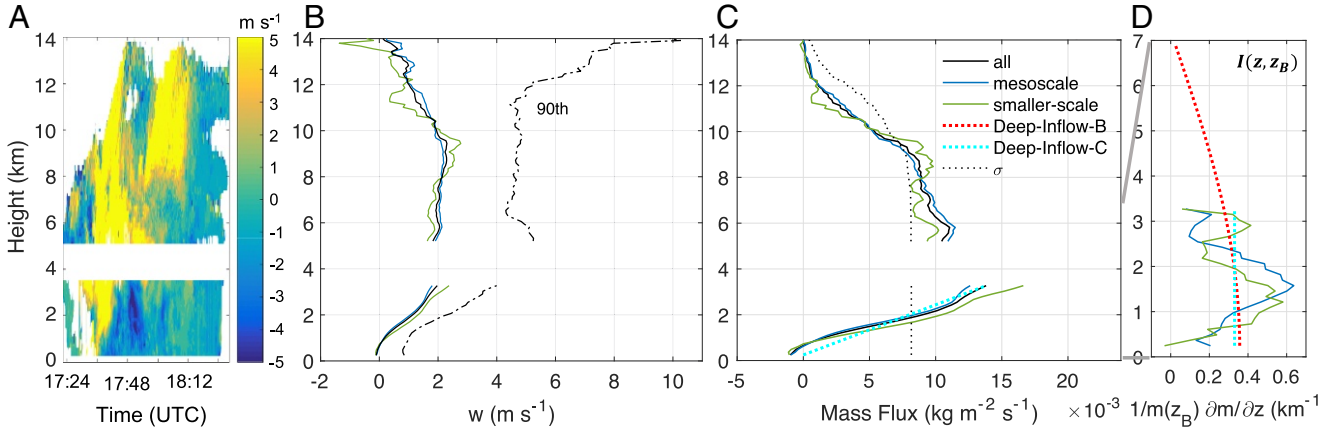

Fig. 1. (*A*) Example updraft core from radar wind profiler retrievals of vertical velocity on April 14, 2014. (*B*) Composites of event-average updraft core vertical velocity for smaller-scale deep convection (30 events; green), mesoscale deep convection (70 events; blue), and all independent deep convective events sampled (mesoscale plus smaller scale, 100 events; black); the black dashed line is the 90th percentile of all composited 1-min profiles. (*C*) As in *B*, but for mean mass flux profile estimates for mesoscale, smaller-scale, and all events. An idealized mass flux profile for Deep-Inflow-C is overlaid. Dashed line shows the convective fraction σ. (*D*) Influence function (Eq. **1**, shown for $z_B \approx 3.3$ km) for the weighting of the environmental variable using the observed mass flux profile for mesoscale and smaller-scale convection and for the Deep-Inflow-B and Deep-Inflow-C idealized mass flux profiles.

dimensions between 50 km and 100 km are excluded here to more clearly distinguish typical mesoscale/smaller-scale profiles from the spectrum of organization. Although sample size precludes more detailed distinction, the smaller-size category commonly includes individual convective cells (see Fig. S1 for examples of both types). Averages of RWP profiles from both spatial ranges of convection identified with the S-band radar are then composited from event means, defined as the means of all 1-min average vertical velocity profiles meeting the convective core criteria within 45 min of others meeting the same criteria.

Mean vertical velocity and mass flux profiles for 30 smaller-scale and 70 mesoscale cases are shown in Fig. 1 *B* and *C*. The shape of σ for mesoscale and smaller-scale convection is nearly identical to σ for all events, so we simply multiply σ for all events by the means of the vertical velocities for each of the two categories of convection, to infer their mass flux profiles. The mass flux for smaller-scale convection is slightly larger in magnitude throughout the lower troposphere than that for mesoscale convection, but for the purpose of inferring mixing properties, the magnitude of the mass flux is irrelevant. Rather, the shape of the profile and the rate of change of mass flux with height determine the weighting of the inflow of environmental air into the plume. The increase in vertical velocity and mass flux with height in the lower troposphere in Fig. 1*C* is nearly linear and consistent for both mesoscale and smaller-scale events.

Deep-Inflow Mixing

Given this growth of mass flux with height through a deep lower-tropospheric layer for both spatial ranges of convection, we reexamine the assumptions needed to relate the precipitation from these systems to a measure of updraft buoyancy. Traditionally, environmental air is entrained and is assumed to mix locally and completely. This places emphasis on the local gradient of mass flux when computing buoyancy, cloud work function (1), or equivalent quantities in deep convective parameterizations. The heterogeneous internal cloud structure from observations and high-resolution models, however, suggests that the in-cloud mixing is not always in situ (31, 52).

A nonlocal formulation of entrainment instead emphasizes layer-mean properties of the inflow. For a level z_B at which buoyancy is to be evaluated, let $r(z_B)$ be the average over the updraft of a conserved variable (ice–liquid water potential temperature is used here). It is not necessary that this variable be fully mixed, only that the average represents a reasonable proxy for the buoyancy at the updraft scale. Considering increments of inflow mass flux $\frac{\partial m}{\partial z}dz$ (where positive) carrying the environmental value $\tilde{r}$ at the level of inflow z, below z_B, this average is

$$r(z_B) = \frac{1}{m(z_B)} \int_{z_0}^{z_B} \tilde{r} \frac{\partial m}{\partial z} dz = \int_{z_0}^{z_B} I(z_B, z)\tilde{r}(z)dz. \qquad [1]$$

In other words, the contribution of the environmental air entering the plume is weighted by the incremental increase in mass flux m with height $\frac{\partial m}{\partial z}(z)$ normalized by the cumulative mass flux $m(z_B)$. This influence function $I(z_B, z)$ of the inflow environment at z on the updraft-average variable at z_B depends on two levels, akin to a matrix approach (53, 54). It has units of km^{-1} like a traditional entrainment parameter (55), but different vertical structure and interpretation. We estimate it from the radar mass flux data in the approximation that the inflow in mass flux remains in the plume through the lower troposphere through the layer where $\frac{\partial m}{\partial z} > 0$.

The influence functions (Fig. 1*D*) from the observed mass flux profiles exhibit slight variations in which the maximum weighting occurs above the boundary layer (1–2 km). However, the leading behavior in both cases is a deep layer of nearly equal weighting from the boundary layer and lower free troposphere. An approximation as a constant weighting in height (Deep-Inflow-C) and a version (Deep-Inflow-B) that is relatively constant but tapers to zero through a deeper layer, as in ref. 33, are overlain in Fig. 1*D*, with the corresponding mass flux profile for Deep-Inflow-C given in Fig. 1*C* (scaling arbitrary).

The leading approximation $m = cz$ linear in height yields an inflow weighting $I(z_B, z) = z_B^{-1}$, independent of z, with the constant c canceling. The tunable coefficient conventionally associated with entrainment is absent, replaced by the geometric consideration of the depth of the layer through which approximately constant inflow occurs. Differentiating [1] with respect to z_B permits translation to a local mixing coefficient, $\epsilon = m^{-1}\partial m/\partial z$ for reference to other schemes, although we do not need to assume that ϵ is physically well defined, except as contributions to the layer integral. The constant weighting case corresponds to local mixing $\epsilon = z^{-1}$. The integral formulation avoids the singularity, physically clarifies the weighting of the different layers, and most importantly makes clear why **[1]** can be expected to apply for the influence of the environment on mesoscale systems, as schematized in Fig. 2.

Fig. 2 summarizes the deep-inflow framework, building on properties of mesoscale systems depicted in the literature (12), but emphasizing the implied relationship to mixing and its impacts on buoyancy tested here. The framework is agnostic as to whether the environmental air is incorporated into the updraft via coherent inflow or small-scale turbulence. The approximation of I constant with height through the lower troposphere can correspond to turbulent increase or to a vertically coherent inflow as is typical in mesoscale systems. No assumption of an influential initial parcel is needed, and robustness of the integral formulation to incomplete or nonlocal mixing makes it plausible to apply this to systems that include mesoscale organization.

Precipitation as a Function of Buoyancy at the GoAmazon2014/5 Site

A bulk measure of plume buoyancy forms the basis for most deep convective parameterizations, which is strongly sensitive to

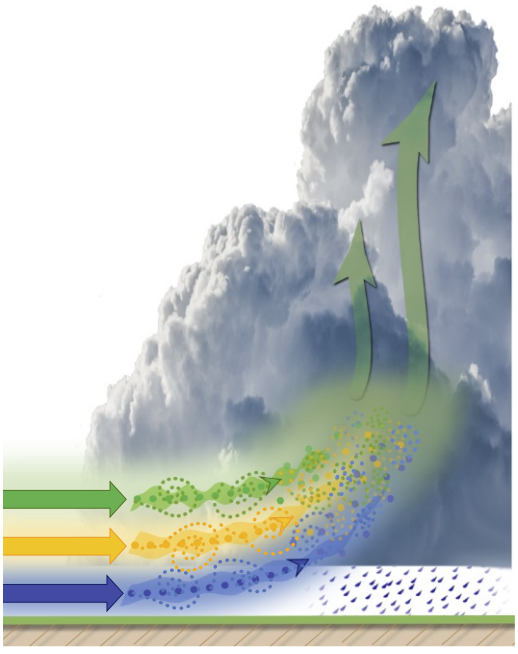

Fig. 2. Schematic of the deep inflow of environmental air into a convecting entity. The inflow can be partly turbulent as has traditionally been assumed for cumulonimbus clouds, and partly coherent as is typical in mesoscale convective systems (12), and is drawn to emphasize the latter. Colors denote an environmental conserved variable entering at different vertical levels at nearly the same rate. These layers therefore contribute similar weighting to the buoyancy computation at a reference level above the inflow layers (Eq. **1**). The inflow layers undergo mixing that is not necessarily local, as depicted by coalescing filaments of environmental air from different layers.

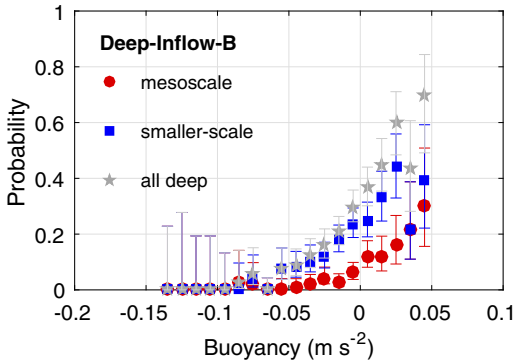

Fig. 3. Probability of observing deep convection (see text for criteria) within 1 h of radiosonde launch, conditionally averaged on 1,000–200 mb mean buoyancy computed with Deep-Inflow-B mixing. Probability is shown for mesoscale and smaller scale convection. Error bars are 5th- to 95th-percentile Wilson score intervals.

mixing assumptions. It is thus of primary interest to relate buoyancy estimated in the inflow mixing framework to the observed deep convective onset of both mesoscale and smaller-scale convection.

Fig. 3 shows the probabilities of deep convection as a function of vertical-mean buoyancy computed using Deep-Inflow-B mixing. Buoyancy $B = g(T_v - \tilde{T}_v)\tilde{T}_v{}^{-1}$ is computed from virtual temperature T_v of the updraft and $\tilde{T}_v$ of the environment using Eq. **1** transformed in pressure coordinates (33), with condensate exceeding 1 g·kg^{-1} removed at each step and condensate frozen below 0 °C. The level z_B at which buoyancy is computed ranges through the troposphere, with the 1,000–200 millibar (mb) average used as a summarizing measure. Deep convective events are defined based on S-band radar precipitation rates averaged over a 100-km box (a typical GCM grid scale) surrounding the GoAmazon2014/5 site exceeding 0.25 mm·h^{-1} and composite reflectivity for at least one point in this domain exceeding 45 dBZ (an indicator of deep convection). The dimension criterion for mesoscale systems is relaxed to 50 km (rather than 100 km) to increase the robustness of the statistics. The sum of the contributions from mesoscale and smaller-scale convection is equal to the total.

A sharp pickup in the probability of deep convective events for both mesoscale and smaller-scale convection is seen in Fig. 3 as a function of updraft buoyancy computed using deep-inflow assumptions. Smaller-scale convective events are more frequent, but both the categories of convection exhibit a similarly strong relationship to precipitation, indicating that buoyancy computed under deep-inflow assumptions is a good predictor of both types of convection. Similar results are obtained using a work function, in which buoyancy is weighted by the mass flux, or using the respective observed influence functions for mesoscale and smaller-scale convection in Fig. 1*D* (Fig. S3). If deep-inflow buoyancy is replaced by convective available potential energy (CAPE), little relation to deep convection is found (Fig. S4) (48, 50), highlighting the importance of a deep-inflow influence function.

Fig. 4 shows conditional averages of precipitation rate as a function of vertical-mean plume buoyancy computed with the four deep-inflow influence functions seen in Fig. 1*D*: two from the empirical estimates from mass flux for mesoscale cases (Deep-Inflow-mesoscale) and smaller-scale cases (Deep-Inflow-smaller scale) and the two approximations to the leading behavior with the influence function constant and constant with a slight taper (Deep-Inflow-C and Deep-Inflow-B, respectively). The similarity of the curves strongly indicates that the variations between the estimated mesoscale and smaller-scale influence functions in Fig. 1*D* have small impact and that the leading behavior controls the buoyancy computation and is insensitive to the assumptions on the level where inflow ends. In this sense, deep-inflow mixing has no remaining substantial parameter dependence. These results are also robust to the layer through which buoyancy is averaged or to using a work function (Fig. S5).

Robustness of Deep-Inflow Assumption across Tropical Land and Ocean Regions

To test whether the deep-inflow mixing assumptions can capture the transition to deep convection in different regions, we use a satellite precipitation-retrieval Tropical Rainfall Measuring Mission (TRMM) Multi-Satellite Precipitation Analysis (TMPA) product 3B42 (TRMM 3B42) at 3-h intervals and 25 km resolution and temperature and moisture from the Interim Reanalysis product (European Centre for Medium-Range Weather Forecasts European Reanalysis; ERA-Interim reanalysis) (*Materials and Methods*).

Fig. 5 presents the conditionally averaged precipitation as a function of vertically averaged buoyancy computed from the Deep-Inflow-B case within different regions of the tropics including four ocean basins and six different land regions. Use of the deep-inflow scheme produces a robust pickup in the precipitation–buoyancy relationship across continental convection regimes. The four ocean basins (Fig. 5*A*) also show rapid increases at nearly the same value of buoyancy. Compared with the tropical oceans, some tropical land regimes show onset at slightly higher values (India and West Africa; Fig. 5*B*) or lower values (South America and Maritime Continent; Fig. 5*C*), while others show precipitation–buoyancy curves in line with the ocean curves (East Asia in Fig. 5*B* and Australia in Fig. 5*C*). Some differences may be noted for heavily precipitating points; these may indicate regional differences for the strongest events but may simply reflect retrieval uncertainties at heavy precipitation.

Discussion

The GoAmazon2014/5 campaign provides an exceptional opportunity to study the interaction between deep convection and the vertically resolved thermodynamic environment. Here, we present a deep-inflow mixing formulation that is compatible with coherent inflow structures of mesoscale convective systems. The coordinated instrumentation permits the evaluation of updraft characteristics of scale-separated convection from radar data and the direct testing of the deep-inflow assumption for its ability to capture deep convective onset.

Empirical evidence for deep-inflow mixing in mesoscale and smaller-scale deep convection is observed in RWP retrievals of vertical velocity and buoyancy–precipitation relations at the GoAmazon2014/5 site. A striking similarity in updraft vertical velocity and mass flux profiles for both forms of deep convection

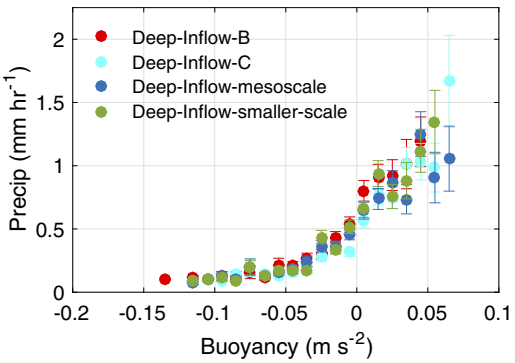

Fig. 4. Precipitation rate (100-km average from S-band radar data ±1 SE) within 1 h of radiosonde launch conditionally averaged on 1,000–200 mb mean buoyancy using the four variants of deep-inflow mixing derived in Fig. 1*D*.

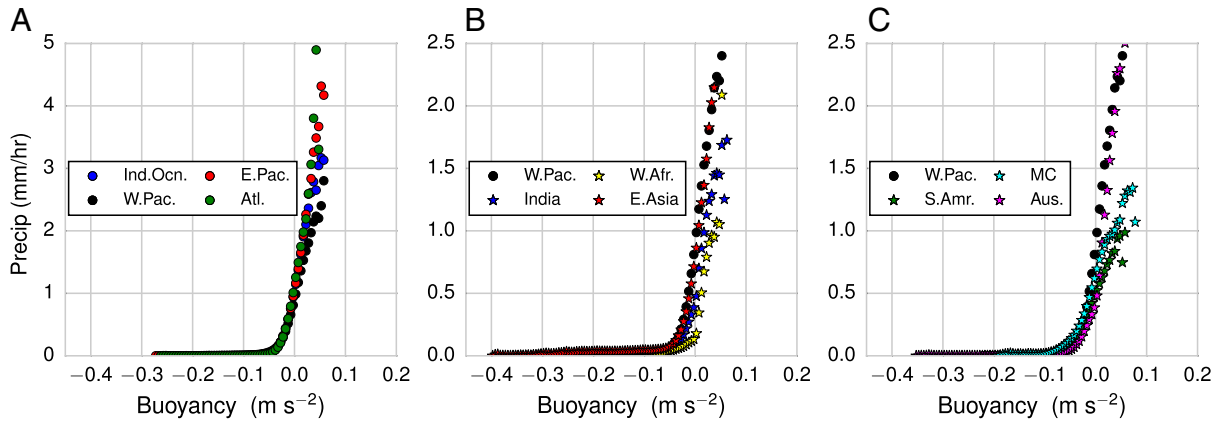

Fig. 5. TRMM 3B42 precipitation conditionally averaged by the mean lower-tropospheric buoyancy (600 mb surface) over different oceanic (*A*) and continental (*B* and *C*) regions of the tropics. Tropical Western Pacific precipitation is used as the reference and is shown as black circles in *B* and *C*. Domains for the regional statistics are as follows: Western Pacific (W.Pac.), 10S–5N, 130E–150E; Indian Ocean (Ind.Ocn), 10S–5N, 70E–90E; Eastern Pacific (E.Pac.), 5N–15N, 240E–260E; Atlantic (Atl.), 5N–15N, 320E–340E; India, 10N–25N, 75E–90E; West Africa (W.Afr.), 10N–20N, 350E–10E; East Asia (E.Asia), 15N–25N, 105E–125E; South America (S.Amr.), 10S–5N, 285E–310E; Maritime Continent (MC), 7S–7N, 95E–145E; and Australia (Aus.), 20S–10S, 125E–145E.

emerges, in which updraft mass flux increases nearly linearly with height throughout the lower troposphere. Influence functions derived from these profiles indicate a leading behavior of relatively constant weighting of environmental variables through this layer.

Buoyancy computed with deep-inflow mixing assumptions exhibits strong relationships to the probability of precipitation and conditional average precipitation from S-band radar. A sharp pickup in both precipitation measures occurs with increasing vertical-mean buoyancy, a relation as strong as or stronger than the relations observed between column-integrated moisture and precipitation (36) at the GoAmazon 2014/5 site. The behavior is robust to variants of deep-inflow mixing and remarkably similar between mesoscale and smaller-scale deep convection.

We interpret this similarity as the two categories of convection—separated by spatial scale—being sustained by the same basic mechanisms driving buoyancy, with the inflow of environmental air into updrafts coming from a roughly comparable deep layer in both cases. The mesoscale systems are commonly preexisting and propagate into the region where the sounding is observed, but the probability of that system continuing to produce precipitation is still controlled by the available buoyancy. Considering inflow through a deep lower tropospheric layer provides a physically intuitive and observationally consistent approach to entrainment that works for conditions supporting both types of convective entities.

In considering applications of the deep-inflow framework to modeling, several caveats should be noted. The onset of conditionally averaged precipitation begins at slightly negative values of lower-troposphere integrated buoyancy. This could be due to sampling mismatches between precipitation and the thermodynamic field or could point to influence of effects beyond the buoyancy considerations here that should be incorporated, including cold pool activation energy (56), updraft contributions recycled from the cloudy environment (31), lifecycle and propagation effects (16–18), or precipitation from less intense convection or stratiform rain. The deep-inflow structure is representative of deep convection and may not be directly transferable to shallow or congestus-type convection, in which coherent structures may play a less dominant role.

Examination of the precipitation–buoyancy relationship with TRMM 3B42 precipitation and thermodynamic profiles from ERA-I reanalysis confirms that deep-inflow assumptions can robustly predict deep convective onset for tropical land and ocean regions alike. The use of a deep-inflow–based buoyancy captures the well-documented sensitivity of tropical convection to free tropospheric humidity as well the influence of the boundary layer.

Implications

These results suggest that two of the key challenges faced by climate model convective parameterizations—representing the effects of MCS convection and sensitivity to poorly constrained entrainment—may be linked. The influence functions estimated here were motivated by seeking a buoyancy computation that could usefully apply to deep convection associated with mesoscale systems. The similarity of deep-inflow estimates between smaller-scale and mesoscale systems suggests commonalities in representing precipitation production in both types of convective entities. The deep-inflow mixing estimated here suggests broader physical interpretations than traditional entraining plume formulations—in particular, consistency with the inclusion of coherent inflow—yet could be implemented within existing formulations. For the conditions of interest here, meeting deep convective criterion and testing for a relationship to strong precipitation, the influence of the environment is comparable for mesoscale and smaller-scale systems and is strong through the inflow layer. The deep-inflow formulation, derived from vertical mass flux estimates, potentially eliminates a leading parameter sensitivity in conventional parameterizations, while showing predictive capability for the probability and magnitude of precipitation as a function of buoyancy.

Materials and Methods

Radar data from the GoAmazon2014/5 field campaign are from the DOE ARM Mobile Facility (March 2014–October 2015) near Manacapuru, Brazil (site T3, 3.21°S, 60.60°W, 50-m altitude) (57). Profiles of vertical velocity and radar reflectivity are from a 1,290-MHz RWP reconfigured for precipitation modes, with a vertical resolution of about 200 m (48) and beam width of ≈1 km below 10 km altitude. S-band radar data are from a system based at Manaus, Brazil at site T1 (3.15°S, 59.99°W). Rain rates are from base (2.5 km) reflectivity using the reflectivity–rain rate (Z-R) relation $z = 174.8R^{1.56}$ derived from disdrometer data. These data are averaged within a 100-km grid box around site T3, but shifted slightly east of center due to data quality outside a 110-km radius of the radar. Composite (i.e., vertical maximum) reflectivity is used to distinguish mesoscale from smaller-scale convection within a 100-km grid box centered on T3.

Thermodynamic profiles are from radiosondes at the T3 site (launched 0130 hours, 0730 hours, 1030 hours; wet season only, 1330 hours and 1930 hours local time), interpolated to 5-mb intervals for mixing computations. Profiles are excluded if rain occurred at T3 $\leq$ 4 h before to avoid

sampling within a cold pool or an environment modified by prior precipitation processes (58). Conditional probability and conditional-average precipitation are computed at 0.02-ms^{-2} intervals in Figs. 3 and 4, for intervals with a minimum of 10 counts total, including nonprecipitating values. In the larger datasets in Fig. 5, 0.005-ms^{-2} intervals and 100-count minimum are used.

The TRMM 3B42 (59) is on a 0.25° grid, based on satellite snapshots within 3-h intervals. Temperature and moisture are from the European Center for Medium Range Weather Forecast (ECMWF) ERA-Interim product (60) on a 0.25° grid and at 6-h intervals. The ERA-I data were horizontally regridded to match the TRMM 3B42 grid and interpolated to 5 mb vertical resolution. TRMM 3B42 data were used at intervals corresponding to the ERA-I data, during September 2001–December 2014.

ACKNOWLEDGMENTS. K.A.S., J.D.N., and F.A. were supported in part by the Office of Biological and Environmental Research of the US Department of Energy (DOE) Grant DE-SC0011074, National Science Foundation Grant AGS-1505198, National Oceanic and Atmospheric Administration Grant NA14OAR4310274, and a Dissertation Year Fellowship from the University of California, Los Angeles (to K.A.S.). Part of this work was performed at the Jet Propulsion Laboratory. The DOE ARM Climate Research Facility field campaign data were essential to this work. S.E.G. of Brookhaven Science Associates, LLC, is supported under Contract DE-SC0012704 with the US DOE.

1. Arakawa A, Schubert WH (1974) Interaction of a cumulus cloud ensemble with the large-scale environment, Part I. *J Atmos Sci* 31:674–701.
2. Kain JS, Fritsch JM (1990) A one-dimensional entraining/detraining plume model and its application in convective parameterization. *J Atmos Sci* 47:2784–2802.
3. Zhang GJ, McFarlane NA (1995) Sensitivity of climate simulations to the parameterization of cumulus convection in the Canadian climate centre general circulation model. *Atmos Ocean* 33:407–446.
4. Bechtold P, et al. (2008) Advances in simulating atmospheric variability with the ECMWF model: From synoptic to decadal time-scales. *Q J R Meteorol Soc* 134:1337–1351.
5. De Rooy WC, et al. (2013) Entrainment and detrainment in cumulus convection: An overview. *Q J R Meteorol Soc* 139:1–19.
6. Tokioka T, Yamazaki K, Kitoh A, Ose T (1988) The equatorial 30-60 day oscillation and the Arakawa-Schubert penetrative cumulus parameterization. *J Meteorol Soc Jpn Ser* 66:883–901.
7. Kim D, et al. (2014) Process-oriented MJO simulation diagnostic: Moisture sensitivity of simulated convection. *J Clim* 27:5379–5395.
8. Knight CG, et al. (2007) Association of parameter, software, and hardware variation with large-scale behavior across 57,000 climate models. *Proc Natl Acad Sci USA* 104:12259–12264.
9. Sanderson BM (2011) A multimodel study of parametric uncertainty in predictions of climate response to rising greenhouse gas concentrations. *J Clim* 24:1362–1377.
10. Sherwood SC, Bony S, Dufresne JL (2014) Spread in model climate sensitivity traced to atmospheric convective mixing. *Nature* 505:37–42.
11. Bernstein DN, Neelin JD (2016) Identifying sensitive ranges in global warming precipitation change dependence on convective parameters. *Geophys Res Lett* 43:5841–5850.
12. Houze RA (2004) Mesoscale convective systems. *Rev Geophys* 42:RG4003.
13. Mapes BE, Houze RA, Jr (1995) Diabatic divergence profiles in western Pacific mesoscale convective systems. *J Atmos Sci* 52:1807–1828.
14. Schumacher C, Houze RA, Jr (2003) Stratiform rain in the tropics as seen by the TRMM precipitation radar. *J Clim* 16:1739–1756.
15. Moncrieff MW (2004) Analytic representation of the large-scale organization of tropical convection. *J Atmos Sci* 61:1521–1538.
16. Mapes B, Neale R (2011) Parameterizing convective organization to escape the entrainment dilemma. *J Adv Model Earth Syst* 3:M06004.
17. Khouider B, Moncrieff MW (2015) Organized convection parameterization for the ITCZ. *J Atmos Sci* 72:3073–3096.
18. Moncrieff MW, Liu C, Bogenschutz P (2017) Simulation, modeling, and dynamically based parameterization of organized tropical convection for global climate models. *J Atmos Sci* 74:1363–1380.
19. Laing AG, Michael Fritsch J (1997) The global population of mesoscale convective complexes. *Q J R Meteorol Soc* 123:389–405.
20. Nesbitt SW, Cifelli R, Rutledge SA (2006) Storm morphology and rainfall characteristics of TRMM precipitation features. *Mon Weather Rev* 134:2702–2721.
21. Mapes B, Tulich S, Lin J, Zuidema P (2006) The mesoscale convection life cycle: Building block or prototype for large-scale tropical waves? *Dyn Atmos Oceans* 42:3–29.
22. Bister M, Emanuel KA (1997) The genesis of Hurricane Guillermo: TEXMEX analyses and a modeling study. *Mon Weather Rev* 125:2662–2682.
23. Houze RA (1997) Stratiform precipitation in regions of convection: A meteorological paradox? *Bull Am Meteorol Soc* 78:2179–2196.
24. Moncrieff MW (1992) Organized convective systems: Archetypal dynamical models, mass and momentum flux theory, and parametrization. *Q J R Meteorol Soc* 118:819–850.
25. Moncrieff MW (2010) The multiscale organization of moist convection and the intersection of weather and climate. *Climate Dynamics: Why Does Climate Vary?*, Geophysical Monograph Series, eds Sun D-Z, Bryan F (American Geophysical Union, Washington, DC), Vol 189, pp 3–26.
26. Randall D, Khairoutdinov M, Arakawa A, Grabowski W (2003) Breaking the cloud parameterization deadlock. *Bull Am Meteorol Soc* 84:1547–1564.
27. Ferrier BS, Houze RA, Jr (1989) One-dimensional time-dependent modeling of GATE cumulonimbus convection. *J Atmos Sci* 46:330–352.
28. Zipser E (1977) Mesoscale and convective–scale downdrafts as distinct components of squall-line structure. *Mon Weather Rev* 105:1568–1589.
29. Kingsmill DE, Houze RA (1999) Kinematic characteristics of air flowing into and out of precipitating convection over the west Pacific warm pool: An airborne Doppler radar survey. *Q J R Meteorol Soc* 125:1165–1207.
30. Mechem DB, Houze RA, Chen SS (2002) Layer inflow into precipitating convection over the western tropical Pacific. *Q J R Meteorol Soc* 128:1997–2030.
31. Yeo K, Romps DM (2013) Measurement of convective entrainment using Lagrangian particles. *J Atmos Sci* 70:266–277.
32. McGee CJ, van den Heever SC (2014) Latent heating and mixing due to entrainment in tropical deep convection. *J Atmos Sci* 71:816–832.
33. Holloway CE, Neelin JD (2009) Moisture vertical structure, column water vapor, and tropical deep convection. *J Atmos Sci* 66:1665–1683.
34. Brown RG, Zhang C (1997) Variability of midtropospheric moisture and its effect on cloud-top height distribution during TOGA COARE. *J Atmos Sci* 54:2760–2774.
35. Zhang Y, Klein SA (2010) Mechanisms affecting the transition from shallow to deep convection over land: Inferences from observations of the diurnal cycle collected at the ARM southern great plains site. *J Atmos Sci* 67:2943–2959.
36. Schiro KA, Neelin JD, Adams DK, Lintner BR (2016) Deep convection and column water vapor over tropical land versus tropical ocean: A comparison between the Amazon and the tropical western Pacific. *J Atmos Sci* 73:4043–4063.
37. Derbyshire S, et al. (2004) Sensitivity of moist convection to environmental humidity. *Q J R Meteorol Soc* 130:3055–3079.
38. Bretherton CS, Peters ME, Back LE (2004) Relationships between water vapor path and precipitation over the tropical oceans. *J Clim* 17:1517–1528.
39. Peters O, Neelin JD (2006) Critical phenomena in atmospheric precipitation. *Nat Phys* 2:393–396.
40. Neelin JD, Peters O, Hales K (2009) The transition to strong convection. *J Atmos Sci* 66:2367–2384.
41. Sahany S, Neelin JD, Hales K, Neale RB (2012) Temperature–moisture dependence of the deep convective transition as a constraint on entrainment in climate models. *J Atmos Sci* 69:1340–1358.
42. Ahmed F, Schumacher C (2015) Convective and stratiform components of the precipitation-moisture relationship. *Geophys Res Lett* 42:10453–10462.
43. Ahmed F, Schumacher C (2017) Geographical differences in the tropical precipitation-moisture relationship and rain intensity onset. *Geophys Res Lett* 44:1114–1122.
44. Giangrande SE, et al. (2017) Cloud characteristics, thermodynamic controls and radiative impacts during the observations and modeling of the green ocean Amazon (GoAmazon2014/5) experiment. *Atmos Chem Phys* 17:14519–14541.
45. LeMone MA, Zipser EJ (1980) Cumulonimbus vertical velocity events in GATE. Part I: Diameter, intensity and mass flux. *J Atmos Sci* 37:2444–2457.
46. May PT, Rajopadhyaya DK (1999) Vertical velocity characteristics of deep convection over Darwin, Australia. *Mon Weather Rev* 127:1056–1071.
47. Kumar VV, Jakob C, Protat A, Williams CR, May PT (2015) Mass-flux characteristics of tropical cumulus clouds from wind profiler observations at Darwin, Australia. *J Atmos Sci* 72:1837–1855.
48. Giangrande SE, et al. (2016) Convective cloud vertical velocity and mass-flux characteristics from radar wind profiler observations during GoAmazon2014/5. *J Geophys Res Atmos* 121:12891–12913.
49. Giangrande SE, et al. (2013) A summary of convective-core vertical velocity properties using ARM UHF wind profilers in Oklahoma. *J Appl Meteorol Climatol* 52:2278–2295.
50. Fan J, et al. (2018) Substantial convection and precipitation enhancements by ultrafine aerosol particles. *Science* 359:411–418.
51. Heymsfield GM, Tian L, Heymsfield AJ, Li L, Guimond S (2010) Characteristics of deep tropical and subtropical convection from nadir-viewing high-altitude airborne Doppler radar. *J Atmos Sci* 67:285–308.
52. Romps DM (2010) A direct measure of entrainment. *J Atmos Sci* 67:1908–1927.
53. Larson VE (1999) The relationship between the transilient matrix and the Green's function for the advection-diffusion equation. *J Atmos Sci* 56:2447–2453.
54. Romps DM, Kuang Z (2011) A transilient matrix for moist convection. *J Atmos Sci* 68:2009–2025.
55. Emanuel KA (1994) *Atmospheric Convection* (Oxford Univ Press, New York).
56. Jeevanjee N, Romps DM (2015) Effective buoyancy, inertial pressure, and the mechanical generation of boundary layer mass flux by cold pools. *J Atmos Sci* 72:3199–3213.
57. Martin S, et al. (2016) Introduction: Observations and modeling of the green ocean Amazon (GoAmazon2014/5). *Atmos Chem Phys* 16:4785–4797.
58. Schiro KA, Neelin JD (2018) Tropical continental downdraft characteristics: Mesoscale systems versus unorganized convection. *Atmos Chem Phys* 18:1997–2010.
59. Huffman GJ, et al. (2007) The TRMM multisatellite precipitation analysis (TMPA): Quasi-global, multiyear, combined-sensor precipitation estimates at fine scales. *J Hydrometeorol* 8:38–55.
60. Dee DP, et al. (2011) The ERA-Interim reanalysis: Configuration and performance of the data assimilation system. *Q J R Meteorol Soc* 137:553–597.